

**Cite this article as:** Cao Jiangdong, Jiang Bochen, Cao Xueyu, et al. Microstructure Evolution of Nickel-based Superalloy GH202 After High Temperature Oxidation from 800 °C to 1100 °C[J]. Rare Metal Materials and Engineering, 2021, 50(12): 4288-4295.

ARTICLE

# Microstructure Evolution of Nickel-based Superalloy GH202 After High Temperature Oxidation from 800 °C to 1100 °C

**Cao Jiangdong<sup>1,2</sup>, Jiang Bochen<sup>1</sup>, Cao Xueyu<sup>1</sup>, Xia Yuyue<sup>1</sup>, Huang Jian<sup>1</sup>, Yao Da<sup>1</sup>**

<sup>1</sup> School of Intelligent Manufacturing and Information, Jiangsu Shipping College, Nantong 226010, China; <sup>2</sup> Jiangsu Tenesun Co., Ltd, Nantong 226010, China

**Abstract:** Microstructure evolution of Ni-based superalloy GH202 after oxidation from 800 °C to 1100 °C was investigated. The results show that the hardness of GH202 decreases with the increase of oxidation temperature, and the hardness is decreased by 43.5% after oxidation at 1100 °C for 100 h. The growth rate of the grains after oxidation at 800 and 900 °C is slower and the grains increase slightly at 900 °C. The grain size increases significantly after oxidation at 1000 and 1100 °C, and many fine grains are annexed to form large grains due to grain boundary migration and elemental diffusion during the recrystallization at high temperatures for above 100 h. The big block carbides (MC) decompose into a large number of carbon atoms which combine with Cr atoms to form a few Cr-rich granular  $M_{23}C_6$ . After oxidation at 900 °C for 150 h, the  $M_{23}C_6$  evolves into Ti-rich  $M_6C$ . With the increase of oxidation temperature, the carbides almost melt into  $\gamma$  phase. Moreover, the  $\gamma'$  phase gradually grows up after oxidation at 800, 900 and 1000 °C, and it is completely dissolved into the  $\gamma$  phase after oxidation at 1100 °C for 100 h.

**Key words:** superalloy; microstructure; high temperature oxidation; carbide; strengthening phase

Superalloys are widely used in the hot end components of aero engines and various gas turbines, such as turbine blades, guide blades, turbine disc, and combustion chambers<sup>[1,2]</sup>. With the increase of engine thrust and thrust-weight ratio, the temperature of the turbine inlet continues to rise. The change of microstructure and the decline of mechanical properties caused by high temperature lead to the reduction of component life<sup>[3]</sup>. This requires higher temperature bearing capacity of superalloys. Therefore, many scholars have designed the composition and process of the superalloy to improve the high temperature bearing capacity of superalloys.

Hundreds of Ni-based superalloys have been developed in the world, which rely mainly on  $Cr_2O_3$  or  $Al_2O_3$  films on the surface to protect the substrate from oxygen penetrating at the high temperature<sup>[4,5]</sup>. Gao et al<sup>[6]</sup> found that the content of Ni in  $\gamma'$ -strengthened Co-based superalloys can promote the formation of protective spinel oxide scales and delay nodular oxidation. Park et al<sup>[7]</sup> revealed that the increase of Al content and addition of Ta are conducive to the formation of

continuous  $Al_2O_3$  and improve the high temperature oxidation resistance of superalloys. Yu et al<sup>[8]</sup> proposed the oxidation mechanism of a novel cobalt-nickel-based superalloy due to evaporation of Mo-containing oxides which result in the formation of voids and roughening of oxides. An et al<sup>[9]</sup> studied evolution of microstructures and properties of GH4169, and the  $\gamma'$ ,  $\gamma''$  phases and carbides dissolving in the grains decrease the tensile strength and increase the ductility. Hu et al<sup>[10]</sup> revealed the four-layer oxide film of a single crystal nickel-based superalloy, in which the diffusion of Ni, Cr and Ta through the alumina layer controls the oxidation. In order to improve the resistance of high temperature oxidation, the selective laser melting<sup>[11]</sup>, ion implantation<sup>[12]</sup>, electron beam<sup>[13]</sup>, laser shock processing<sup>[14]</sup> etc are used to change the microstructure and composition of the surface. However, more attention has been paid to the microstructure changes of oxide films on the surface rather than the microstructure evolution of matrix.

In this work, the evolution of carbides, strengthening

Received date: May 02, 2021

Foundation item: Natural Science Foundation of Jiangsu Province (BK20191204); Natural Science Foundation of Jiangsu Province for Universities and Colleges (19KJB430031)

Corresponding author: Cao Jiangdong, Ph. D., Professor, School of Intelligent Manufacturing and Information, Jiangsu Shipping College, Nantong 226010, P. R. China, Tel: 0086-513-85965529, E-mail: caojd@jssc.edu.cn

Copyright © 2021, Northwest Institute for Nonferrous Metal Research. Published by Science Press. All rights reserved.

phases and grains in Ni-based superalloy GH202 after oxidation from 800 °C to 1100 °C was investigated. The microstructures of the alloy before and after high temperature oxidation were characterized by TEM (transmission electron microscope), SEM (scanning electron microscope) and EBSD (electron backscatter diffraction). The effect of high temperature oxidation on the microstructures was discussed from the aspects of grain size, orientation distribution, recrystallization and stress, which may provide an important reference for the application and development of superalloys.

## 1 Experiment

### 1.1 Materials and the specimen preparation

Ni-based superalloy GH202 is usually used in the rotors and stators of the large thrust liquid rocket engines. The melting point of the alloy is 1317~1342 °C, and the hardness is about 3560 MPa after the solution strengthening and aging treatment.

The Ni-based superalloy GH202 was cut into a cuboid specimen (10 mm×10 mm×5 mm) by a wire cut electric discharge machine. The surface of the specimens was ground to 1200# on the SiC sandpaper and polished on the machine with nylon. The specimens were soaked in acetone, alcohol, and deionized water successively, then cleaned by ultrasonic wave, and finally they were dried by a blower.

The strengthening phases ( $\gamma'$ ), twins and dislocations of the superalloy were characterized by TEM (transmission electron microscope). Scanning electron microscope (SEM) with energy dispersive spectrometer (EDS) was used to analyze the

morphology and chemical composition of the superalloy before and after high temperature oxidation. The grain orientation, grain size distribution, recrystallization, and stress were characterized by EBSD (electron backscatter diffraction). Hardness tests were performed on a micro-hardness tester (HV-1000), with a load of 200 g and dwelling time of 15 s at room temperature.

### 1.2 High temperature oxidation experiment

The  $\text{Al}_2\text{O}_3$  crucibles were put into the box-type furnace at 600 °C and impurities were removed. All the specimens were placed in the  $\text{Al}_2\text{O}_3$  crucibles and kept in linear contact with side walls. The isothermal oxidation experiments of the specimens were carried out in a box furnace at 800, 900, and 1000 °C for 150 h, and 1100 °C for 100 h. After high temperature oxidation, the specimens were taken out of the furnace and cooled down to room temperature.

### 1.3 Microstructure analysis

The grain orientation distribution of Ni-based superalloy GH202 is shown in Fig. 1a, and different colors represent different orientations of the grains. There are a few small grains below 10~20  $\mu\text{m}$  among the boundaries of larger grains with the size over 30  $\mu\text{m}$ , as shown in Fig. 1b, and some annealing twins exist in the grains. With the EDS test, the chemical composition of the superalloy is shown in Fig. 1c. The carbides exist at the grain boundaries in the form of bulks and chains, as shown in Fig. 1d.

Fig. 2 shows the TEM images of Ni-based superalloy GH202 treated by the solution strengthening. The strengthening phases ( $\gamma'$ ) exist as a sphere or ellipsoid with a

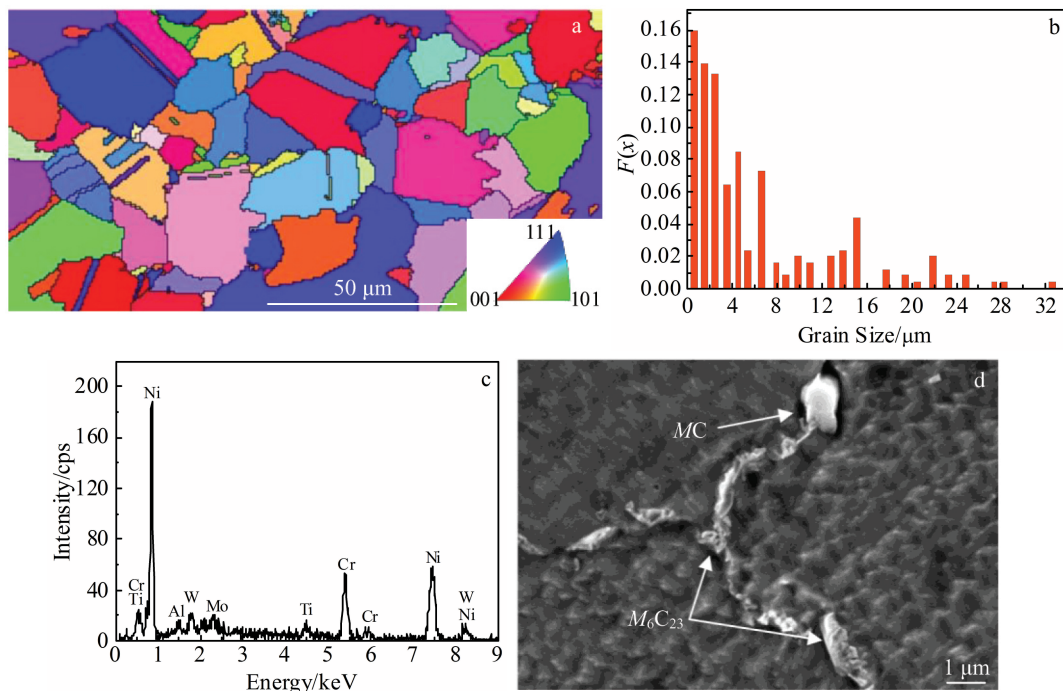


Fig.1 EBSD mapping of grains (a), grain size distribution (b), EDS spectrum analysis (c), and carbides at the grain boundaries (d) for Ni-based superalloy GH202 treated by the solution strengthening before oxidation

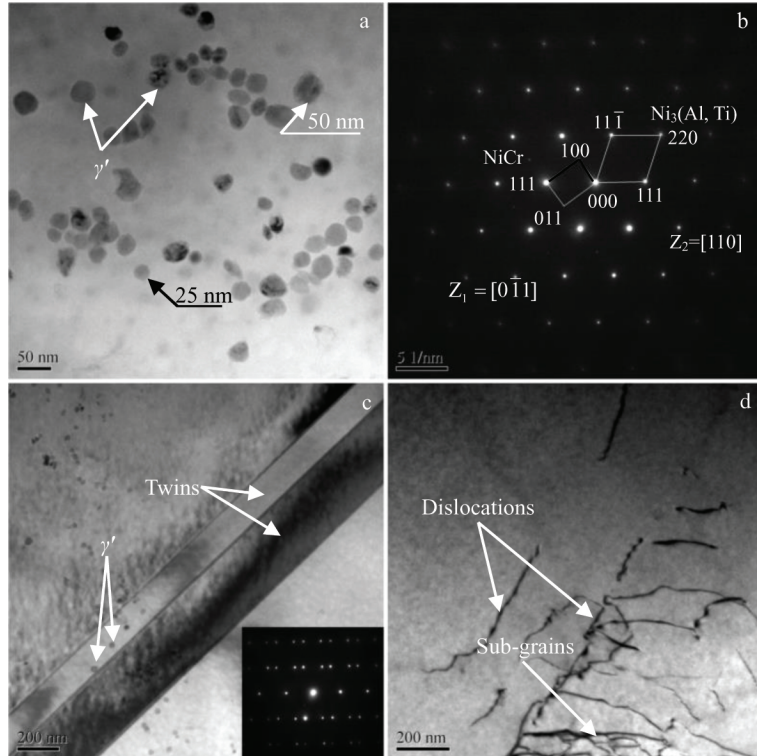


Fig.2 TEM images of Ni-based superalloy GH202: (a)  $\gamma'$ , (c) twins, and (d) dislocations; SAED pattern of  $\gamma$  and  $\gamma'$  (b)

diameter of 20~50 nm in Fig.2a. From the SAED pattern in Fig.2b, it can be seen that there are two sets of spots, one is a NiCr solid solution and the other is precipitated phase  $\text{Ni}_3(\text{Al}, \text{Ti})$ . A few annealing twins exist in the superalloy according to the double point diffracted spot in Fig.2c. A small amount of sub-grains dislocation lines are produced due to heat treatment in Fig.2d.

## 2 Results and Discussion

### 2.1 Surface morphology after oxidation

Fig. 3 shows the oxidation film morphology and selected point EDS analysis of the Ni-based superalloys after oxidation from 800 °C to 1100 °C. According to Ref.[15], the dense and continuous oxidation film is mainly composed of  $\text{Cr}_2\text{O}_3$  as shown in Fig.3a and EDS results are shown in Fig.3e, which can protect oxygen from penetrating into the superalloy. With the increase of temperature, the oxides grow up obviously at 900 °C, and some small holes appear in the film in Fig.3b. After oxidation at 1000 °C for 150 h, the oxidation film is peeled off in some zones in Fig.3c, and  $\text{TiO}_2$  grows up to make the oxide film loose due to  $\text{Ti}^{4+}$  diffusing to the surface (as seen in Fig.3f). The large spallation of the film occurs at 1100 °C for 100 h in Fig.3d, and a new oxidation film is formed.

### 2.2 Effect of high temperature oxidation on hardness of the superalloy

Fig.4 shows the changes of the Vickers hardness before and after oxidation from 800 °C to 1100 °C. The hardness of the substrate shows a declining trend from the room temperature,

and it is 3560, 3230, 2720, 2550, and 2010 MPa from sample 1 to sample 5, respectively. It can be seen that the hardness changes greatly after oxidation from 800 °C to 900 °C and from 1000 °C to 1100 °C, and it is decreased by 43.5% after oxidation for 100 h at 1100 °C. Therefore, high temperature oxidation has a great influence on the mechanical properties of the Ni-based superalloys.

### 2.3 Microstructure changes after high temperature oxidation

Fig.5 shows the grain orientation and size of the Ni-based superalloys after high temperature oxidation from 800 °C to 1100 °C. The grain orientation is not consistent in Fig.5a, 5c, 5e and 5g, indicating that the material is isotropic before and after high temperature oxidation. There are a large number of twins in all specimens. In Fig.5b and 5d, the grain size does not increase significantly after oxidation from 800 °C to 900 °C, and even some grains are refined. In Fig.5f and 5h, the maximum grain size of the superalloy suffering oxidation at 1000 and 1100 °C is up to 93 and 182  $\mu\text{m}$ , respectively, indicating that the grain growth is very significant above 1000 °C.

Fig.6 shows recrystallization and deformation of the grains after the high temperature oxidation from 800 °C to 1100 °C. Most of the grains are recrystallized at high temperatures in Fig. 6a~6d. The number of the sub-grains is the largest compared with that after oxidation at 800, 1000 and 1100 °C. There are many small sub-grains between the larger grains, and they become larger with the increase of the oxidation temperature. A small amount of grains are deformed after

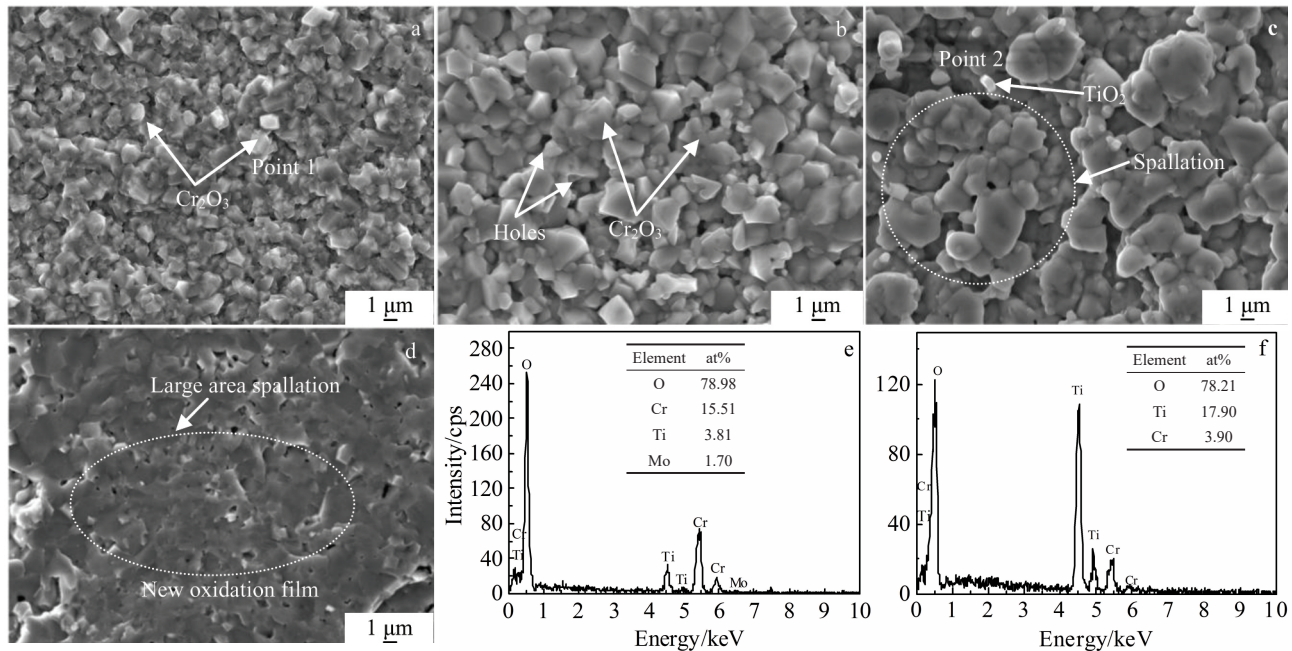


Fig.3 SEM surface morphologies and EDS results of point 1 in Fig.3a (e) and point 2 in Fig.3c (f) after oxidation under different conditions:  
(a) 800 °C for 150 h, (b) 900 °C for 150 h, (c) 1000 °C for 150 h, and (d) 1100 °C for 100 h

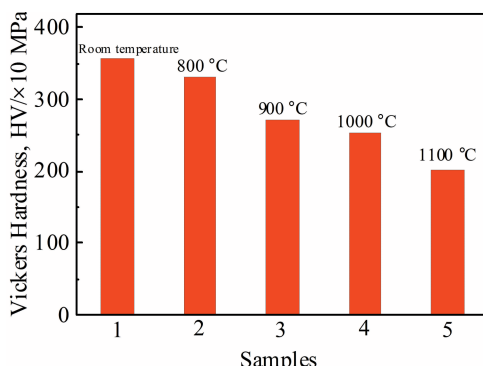


Fig.4 Vickers hardness before and after oxidation

oxidation at 800, 900 and 1000 °C.

Fig. 7 shows the stress among the grains after oxidation from 800 °C to 1100 °C. The red areas represent high stress, and the green areas have relatively small stress. In Fig.7a and 7b, the high stress occurs at the adjacent edges of the multiple grains, and there is also a relatively small stress in the center of some large grains. It is clearly seen that the stressed grains after oxidation at 900 °C are more than that at 800 °C. With the increase of oxidation temperature, the stress of grain decreases gradually.

#### 2.4 Carbides at the grain boundaries after oxidation

Fig.8 shows the SEM images of the grains and carbides at the grain boundaries after high temperature oxidation from 800 °C to 1100 °C. It can be clearly seen from Fig.8a that a large amount of the white carbides are precipitated at grain boundaries after oxidation at 800 °C for 150 h. With the increase of oxidation temperature, the fine grains tend to

increase after oxidation at 900 °C for 150 h, and the carbides continue to precipitate and form large lumps in Fig.8b. The carbides at the boundaries almost disappear due to the dissolution of the carbides ( $M_6C$ ) in the  $\gamma/\gamma'$  phase at 900 and 1000 °C in Fig.8c. After oxidation at 1100 °C, a few small carbides precipitate in the middle of the grains in Fig.8d.

Fig. 9 shows the morphologies and EDS analysis of the carbides in the grain boundaries after oxidation from 800 °C to 1100 °C. It can be seen from Fig.9a that a few carbides at the grain boundary still maintain a continuous chain, and a lot of granular Cr-rich  $M_{23}C_6$  form after oxidation at 800 °C, as shown in Fig.9e. After oxidation at 900 °C for 150 h, the carbides are mainly  $M_6C$ , and its chemical composition is shown in Fig.9f. When the oxidation temperature exceeds 1000 °C, the carbides completely disappear in Fig.9c. Moreover, a small number of inter-crystalline pores appear after oxidation at 1100 °C for 100 h, as shown in Fig.9d.

#### 2.5 Strengthening phase morphologies

Fig. 10 shows the strengthening phase ( $\gamma'$ ) morphologies after oxidation from 800 °C to 1100 °C. With the increase of oxidation temperature, the strengthening phase grows continuously. The diameter of the  $\gamma'$  phase after oxidation at 800, 900 and 1000 °C is about 100, 330 and 480  $\mu$ m in Fig.10a~10c, respectively. After oxidation at 1100 °C for 100 h, the  $\gamma'$  phase is completely dissolved into the  $\gamma$  phase, and it presents a lamellar structure in Fig.10d.

#### 2.6 Discussion on mechanism of microstructure evolution after oxidation

##### 2.6.1 Evolution of the oxidation film

The content of Cr in the Ni-based superalloy GH202

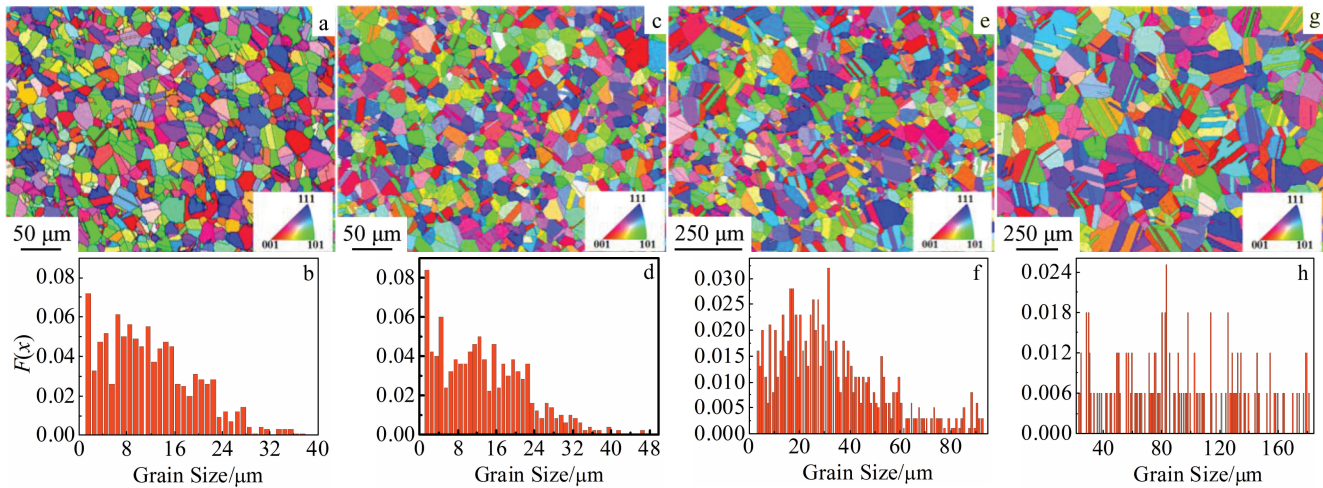


Fig.5 Grain orientation mappings (a, c, e, g) and grain size distribution (b, d, f, h) of Ni-based superalloys after high temperature oxidation: (a, b) 800 °C for 150 h, (c, d) 900 °C for 150 h, (e, f) 1000 °C for 150 h, and (g, h) 1100 °C for 100 h

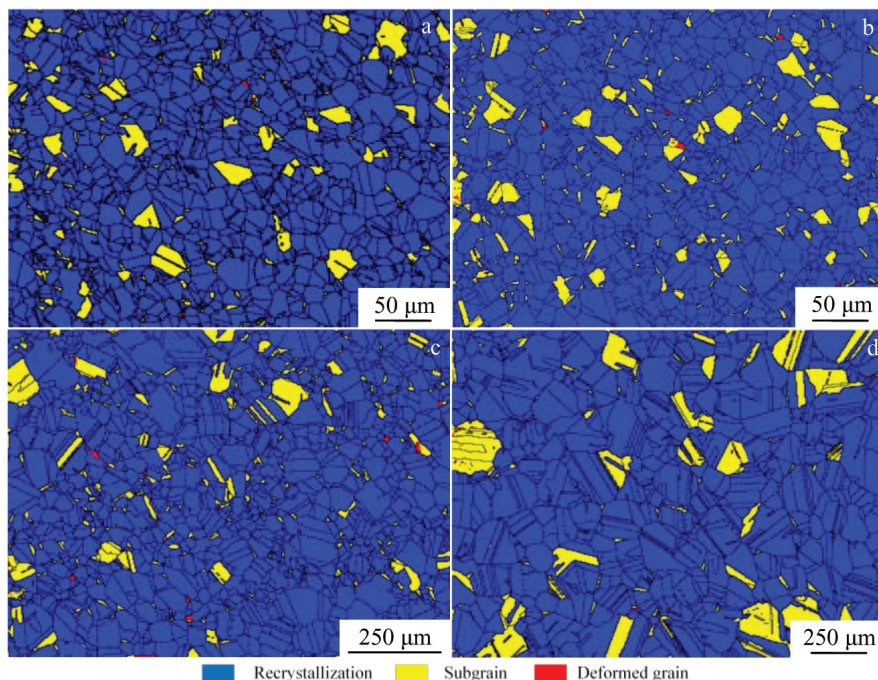
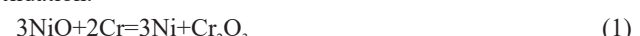


Fig.6 Recrystallization and deformation of the grains after oxidation: (a) 800 °C for 150 h, (b) 900 °C for 150 h, (c) 1000 °C for 150 h, and (d) 1100 °C for 100 h

reaches the critical value, which is favorable for selective oxidation to form a continuous  $\text{Cr}_2\text{O}_3$  oxidation film<sup>[16]</sup>. The element Cr in the alloy has a strong oxygen absorption ability, which can reduce the partial pressure of the oxygen at the alloy/film interface, which is beneficial to the stability of the film. The oxidation rate constant ( $K_p$ ) of  $\text{Cr}_2\text{O}_3$  is several orders of magnitude lower than that of  $\text{NiO}$ , which leads to the replacement reaction of Eq. (1). With the increase of oxidation temperature, the oxide grains grow up further and  $\text{Ti}^{4+}$  diffuses to the surface of the oxide film to form blocky  $\text{TiO}_2$ . Subsequently, the oxide film becomes sparse and

oxygen can penetrate the oxide film to generate the internal oxidation.



## 2.6.2 Evolution of the grains after oxidation

The austenite grains of Ni-based superalloys GH202 exhibit polygonal equiaxed crystal with twins at the room temperature. After oxidation at 800 °C for 150 h, the grains are recrystallized and grow very slightly. There is a tendency of grain refinement after oxidation at 800 °C for 150 h. The grains do not grow up obviously, and the fine grains and subgrains increase due to the rapid cooling of the recrystallization

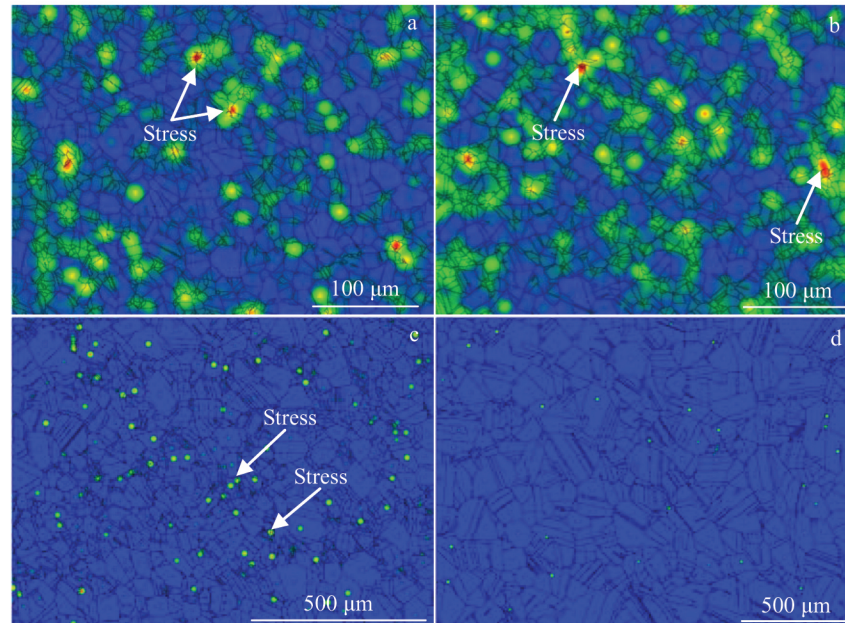


Fig.7 Stress of the grains after oxidation: (a) 800 °C for 150 h, (b) 900 °C for 150 h, (c) 1000 °C for 150 h, and (d) 1100 °C for 100 h

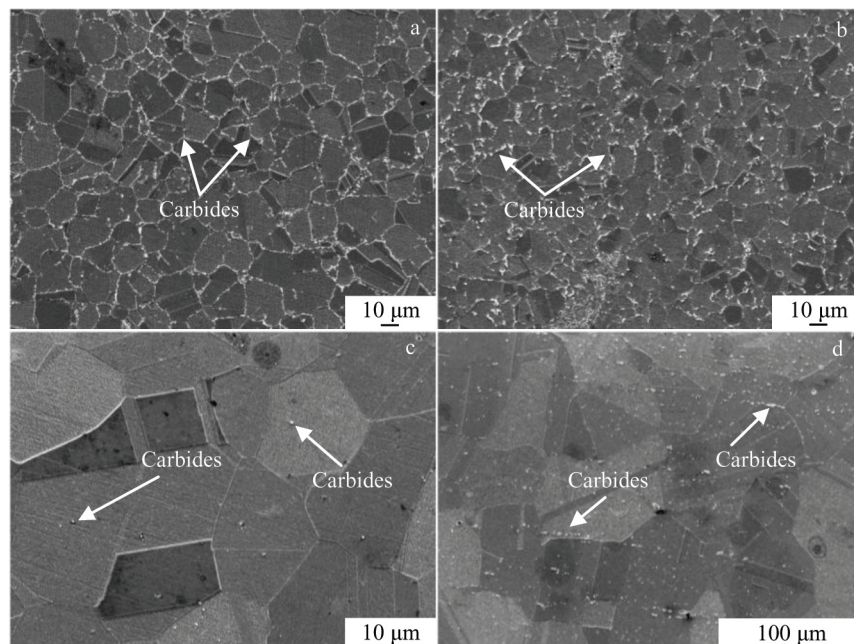


Fig.8 SEM images of the grains and carbides at grain boundaries after oxidation: (a) 800 °C for 150 h, (b) 900 °C for 150 h, (c) 1000 °C for 150 h, and (d) 1100 °C for 100 h

at high temperatures. After oxidation at 1000 and 1100 °C, the austenite grains grow significantly and the edges become straight from bending. The grain size of Ni-based superalloy GH202 before high temperature oxidation is not uniform, and a few fine grains exist among the large grains, which lead to the high interface energy and the instability of grain boundaries according to thermodynamic theory. Under certain conditions, the grain boundary area and interface energy

might decrease spontaneously. In Eq.(2), the driving force ( $F$ ) of austenite grains is related to the radius of the grain boundary and interface energy. The greater driving force ( $F$ ) is produced due to the higher interface energy and the smaller grain size. The grain boundary migration become easier, and the grains grow up<sup>[17-19]</sup>. When the temperature increases, the grain boundaries with small radius of curvature move towards the center of the curvature, which results in the flattening of

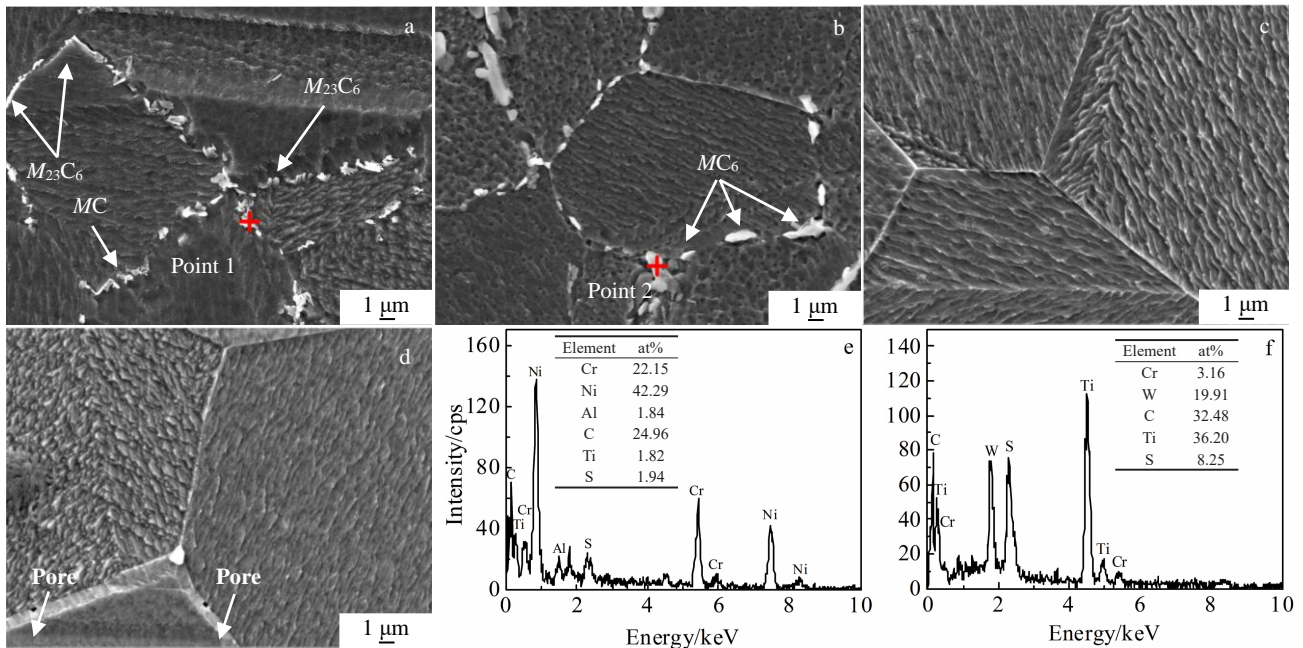


Fig.9 Morphologies and EDS results of point 1 in Fig.9a (e) and point 2 in Fig.9b (f) of the carbides in the grain boundaries after oxidation: (a) 800 °C for 150 h, (b) 900 °C for 150 h, (c) 1000 °C for 150 h, and (d) 1100 °C for 100 h

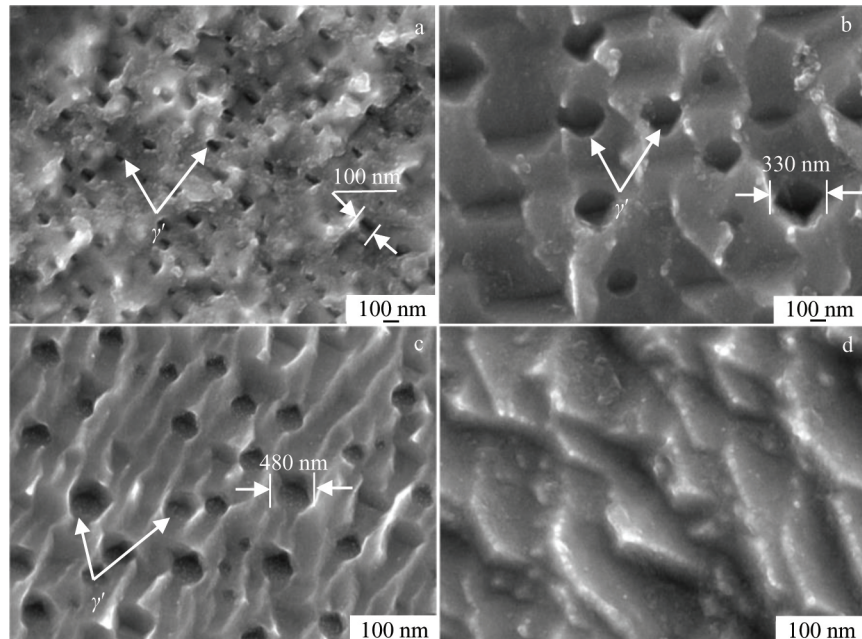


Fig.10 Strengthening phase ( $\gamma'$ ) morphologies after oxidation: (a) 800 °C for 150 h, (b) 900 °C for 150 h, (c) 1000 °C for 150 h, and (d) 1100 °C for 100 h

grain boundaries:

$$F = \frac{2\delta}{R} \quad (2)$$

in which  $F$  represent driving forces of grain boundary migration,  $\delta$  stands for grain boundary interface energy per unit area, and  $R$  is radius of curvature of the grain boundary.

### 2.6.3 Evolution of the carbides

During the solidification of the Ni-based superalloy, a variety of the carbides will be precipitated, such as  $MC$ ,  $M_{23}C_6$ ,  $M_6C$ . Under the condition of high temperature for a long time, the carbides can decompose and degrade<sup>[20]</sup>. A large number of carbon atoms in the carbide ( $MC$ ) are decomposed

and combined with Cr atoms in the  $\gamma$  phase to form the granular  $M_{23}C_6$  at 800 °C<sup>[21,22]</sup>. After oxidation at 900 °C for 150 h, many large blocks of the carbides precipitate at the grain boundaries, which are mainly Ti-rich  $M_6C$  due to the degradation and decomposing of  $M_{23}C_6$  at high temperatures.

### 3 Conclusions

1) For the GH202 superalloy with high temperature oxidation, a large number of fine grains are annexed to form large grains through the grain boundary migration above 1000 °C. The grain boundaries move towards the center of the curvature and become flat.

2) The big block carbides (MC) decompose into a large number of carbon atoms which are combined with Cr atoms to form Cr-rich  $M_{23}C_6$ , and some of them change from the chain shape to the granular shape. After oxidation at 900 °C for 150 h, the  $M_{23}C_6$  evolves into Ti-rich  $M_6C$ . When the temperature is above 1000 °C, the carbides almost disappear.

3) The  $\gamma'$  phase grows up with the increase of temperature, and it is completely dissolved into the  $\gamma$  phase at 1100 °C for 100 h.

4) The hardness of the superalloy GH202 decreases with the increase of oxidation temperature due to the evolution of crystal structure, carbides and  $\gamma'$  phase.

### References

- Guo Y, Zhang J X, Xiong J K. *Rare Metal Materials and Engineering*[J], 2021, 50(4): 1462
- Cao J D, Zhang J S, Hua Y Q et al. *Rare Metals*[J], 2017, 36: 878
- Ioannis Bantounas, Bharat Gwalani, Talukder Alam et al. *Scripta Materialia*[J], 2019, 163: 44
- Saber D, Islam S Emam, Abdel-Karim R. *Journal of Alloys and Compounds*[J], 2017, 719: 133
- Hu Y B, Zhang L, Cheng C Q et al. *Acta Metallurgica Sinica*[J], 2017, 30(9): 857
- Gao B, Wang L, Liu Y et al. *Corrosion Science*[J], 2019, 157: 109
- Park S J, Seo S M, Yoo Y S et al. *Corrosion Science*[J], 2015, 90: 305
- Yu B H, Li Y P, Nie Y et al. *Journal of Alloys and Compounds*[J], 2018, 765: 1148
- An X L, Zhang B, Chu C L et al. *Materials Science & Engineering A*[J], 2019, 744: 255
- Hu Y B, Cheng C Q, Zhang L et al. *Oxidation of Metals*[J], 2018, 89: 303
- Kim K S, Yang S S, Kim M S et al. *Journal of Materials Science & Technology*[J], 2021, 76: 95
- Zschau H E, King F, Galetz M C et al. *Nuclear Instruments and Methods in Physics Research B*[J], 2015, 365: 202
- Zhao L H, Tan Y, Shi S et al. *Vacuum*[J], 2019, 170: 108 979
- Cao J D. *Applied Surface Science*[J], 2019, 493: 729
- Cao J D, Zhang J S, Hua Y Q et al. *Materials Characterization*, 2016, 118: 122
- Athreya C N, Deepak K, Kim Dong-Ik et al. *Journal of Alloys and Compounds*[J], 2019, 778: 224
- Xu M, Liu G H, Zhang X L. *Rare Metal Materials and Engineering*[J], 2021, 50(4): 1350
- Xu C, Nai Q L, Yao Z H et al. *Acta Metallurgica Sinica*[J], 2017, 53: 1453 (in Chinese)
- Olmsted D L, Foiles S M, Holm E A. *Acta Materialia*[J], 2009, 57: 3704
- Joseph C, Persson C, Colliander M Hornqvist. *Metallurgical and Materials Transactions A* [J], 2020, 51: 6136
- Maldonado R, Nembach E. *Acta Materialia*[J], 1997, 45(1): 213
- Hong J K, Park N K, Kim S J et al. *Materials Science Forum*[J], 2005, 502: 249

## 镍基高温合金GH202高温氧化后的微观组织演变

曹将栋<sup>1,2</sup>, 姜伯晨<sup>1</sup>, 曹雪玉<sup>1</sup>, 夏雨乐<sup>1</sup>, 黄健<sup>1</sup>, 姚达<sup>1</sup>

(1. 江苏航运职业技术学院 智能制造与信息学院, 江苏 南通 226010)

(2. 江苏天舒电器有限公司, 江苏 南通 226010)

**摘要:** 研究了镍基高温合金GH202在800~1100 °C高温氧化后晶粒、碳化物和强化相的演变过程。采用透射电子显微镜、扫描电子显微镜和电子背散射衍射对其微观结构进行了表征。结果表明: 镍基高温合金的硬度随氧化温度的升高而降低, 1100 °C氧化100 h后, 硬度降低了43.5%。800和900 °C氧化后晶粒生长速度较慢, 而经900 °C氧化后晶界碳化物析出显著增加。在1000和1100 °C氧化后, 晶粒尺寸明显增大。氧化过程中晶界迁移是由晶界两侧自由能差决定, 温度越高, 晶界向曲率中心迁移越快, 大量细小晶粒被吞并形成了大晶粒。大块状碳化物(MC)分解成大量的碳原子, 与Cr原子结合形成少量的富Cr颗粒状 $M_{23}C_6$ 。在900 °C氧化150 h后,  $M_{23}C_6$ 演化为富Ti的 $M_6C$ 。随着氧化温度的升高, 碳化物在 $\gamma$ 相中回熔。在800、900和1000 °C氧化后,  $\gamma'$ 相逐渐长大, 在1100 °C氧化100 h后, 完全溶解于 $\gamma$ 相。

**关键词:** 高温合金; 微观组织结构; 高温氧化; 碳化物; 强化相

**作者简介:** 曹将栋, 男, 1979年生, 博士, 教授, 江苏航运职业技术学院智能制造与信息学院, 江苏 南通 226010, 电话: 0513-85965529, E-mail: caojd@jssc.edu.cn